ICAS 2020 SHANG HAI
International Council of the Aeronautical Sciences
32nd Congress of the International Council of the Aeronautical Sciences
September 6-10, 2021
Pudong Shangri-La, Shanghai, China

INCREASING THE EFFECTIVENESS OF AN AERODYNAMICALLY BALANCED CONTROL SURFACE ON A MODIFIED AIRFOIL WITH REDUCED DRAG

V. Bogatyrev[1]

[1]Central Aerohydrodynamic Institute (TsAGI), Russia

Abstract

For aircraft flight control, control surfaces are usually employed that represent moveable surfaces at the trailing edges of such aerodynamic surfaces as wings and horizontal and vertical stabilizers. For decreasing the hinge moments of control surfaces, their aerodynamic balances are widely used. As a rule, cross-sectional shapes of aerodynamic surfaces represent streamlined airfoils and, when the control surfaces are installed, the shapes of the forward fixed parts of the aerodynamic surfaces remain unchanged. In the current paper it is showed that small changes in the shapes of the aerodynamic surfaces ahead of control surfaces can improve both aerodynamic-surface aerodynamic perfection and control-surface effectiveness.

Keywords: aerodynamically balanced control surface, effectiveness, drag

1. Introduction

In aircraft design, it is important to find compromise between different aspects including aerodynamic perfection, fuel efficiency, stability and control. As a rule, the best aerodynamic perfection with undeflected controls is achieved for simple control surfaces made with minimal gaps the most common of which have the so-called plain overhang (PO) i.e. the front part of the mentioned control surfaces has a circular cross-section perpendicular to the hinge axis and centered in it. An example of the control surface with the PO is shown in Figure 1(a). Such control surfaces produce a smaller increase in the aerodynamic drag of the aerodynamic surface due to their installation on it but usually require powerful and heavy actuators because of large hinge moments.

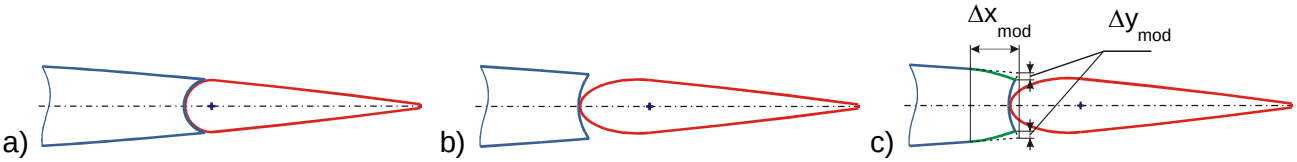

Figure 1 – Control surfaces: (a) with a plain overhang, (b) with an overhang balance, and (c) modification [5].

One of the most simple and common ways to reduce hinge moments of control surfaces is their aerodynamic balancing by use of an overhang balance (OB). The OB represents a part of the control surface located ahead of its hinge line that, due to the pressure difference across the control surface, generates a moment opposite in sign to that one generated behind the hinge line. As a rule, the OB shape is tapered to the front, so that, at moderate control-surface deflection angles, the OB would not project much. For example, Figure 1(b) shows a control surface with an OB, which has an elliptical arc cross-section. This type of OB shape forms bluff edges on the aerodynamic surface in front of the control surface, which contribute to an increase in the aerodynamic drag (e.g., [1,2]).

The control surfaces with OBs are extensively studied. For example, the TsAGI experience in experimental researches of such control surfaces for aircraft with unpowered controls is summarized in [3]. The computational studies of the effect of modifying the shape of the gap between the aerodynamic surface and the control surface were carried out in [4]. The current paper explores

another type of aerodynamic surface modification that is based on the patent [5]. To reduce the drag of the aerodynamic surface having a control surface with an OB, smooth trimming of a small portion of the aerodynamic surface in front of the control surface was proposed, a version of which is shown in Figure 1(c) for the case of limiting the longitudinal and transverse trimming dimensions by the parameters Δx_{mod} and Δy_{mod}, respectively. Some results concerning the drag reduction due to symmetrical trimming of the aerodynamic surface with a NACA 0015 airfoil are presented in [6]. However, it is important to evaluate the change in the control surface effectiveness and hinge moment resulting from the aerodynamic-surface modification. This evaluation is conducted in the current paper.

2. Basic Data

The basic parameters correspond to the aerodynamic surface investigated in [2]. The aerodynamic surface with a symmetric airfoil NACA 0015 has a control surface with an OB. The control-surface chord measured behind the hinge line is 30 percent of the airfoil chord and the OB chord is 50 percent of the control-surface chord. The gap at the nose of the control surface is 0.5 percent of the airfoil chord.

A rectangular wing with a control surface (or simple flap) and specified geometric parameters was tested in the vertical NACA wind tunnel with a closed test section of 4×6 ft (1.22×1.83 m) [2]. The wing chord was equal to 2 ft (0.61 m). The wing was spanned between the walls of the wind tunnel to create conditions close to the two-dimensional (2D) flow. The tests were carried out at Mach number of $M = 0.1$ and Reynolds number of $Re = 1.4 \times 10^6$. The turbulence factor [7,8] defined as the ratio between the critical Reynolds numbers of a sphere in the non-turbulent flow and the wind tunnel flow, during the tests [2], was equal to 1.93 and corresponded to a turbulence intensity of $Tu \approx 1.2\%$. For comparison, the data obtained during the tests of the rectangular wing with the control surface having a PO [1] were also analyzed.

3. Validation

Computational studies of the 3D flow around the wing with control surfaces at $M = 0.1$, $Re = 1.4 \times 10^6$, and $Tu \approx 1.2\%$ were carried out using ANSYS CFX. The computational mesh was generated for the domain with the dimensions proportional to the halved test section of the vertical NACA wind tunnel assuming the symmetrical flow. The domain was scaled up to correspond to the airfoil chord of 3 m. This was done taking into account the possibility of using the same mesh for different Reynolds numbers which may be reached by different pressure levels.

The unstructured mesh had multiple layers spanwise from the central cross section, which was considered to be the plane of symmetry for the flow, to the side wall with the reducing spanwise step near it. Each layer consisted of the same 2D mesh. This 2D mesh had quadrilateral cells and included 48 prism layers near the airfoil walls with the first layer height of 5 μm and the growth rate of 1.1. The examples of the 3D mesh in spanwise layers and of the surface mesh on the aerodynamic surface are shown in Figures 2(a) and 2(b), respectively. The total number of cells in the 3D meshes was about 8 million.

a) 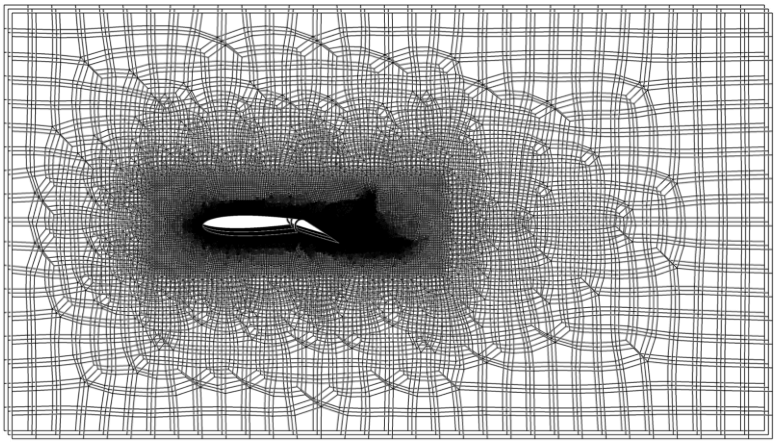 b) 

Figure 2 – Example of a computational 3D mesh: (a) spanwise layers, (b) surface mesh.

Because of the interest in the flow near the airfoil that is not confined by the wind tunnel walls, the 2D external flow was also computed. For this kind of the flow, the 2D meshes had inlet and outlet boundaries as far as about 22 airfoil chords from it. The 2D meshes had the prism layers near the airfoil walls with the same parameters as for the 3D meshes but the 2D meshes were much finer than the meshes in the spanwise layers of the 3D meshes. The size of the 2D meshes was about 1.6 million cells. The example of the 2D mesh is shown in Figure 3.

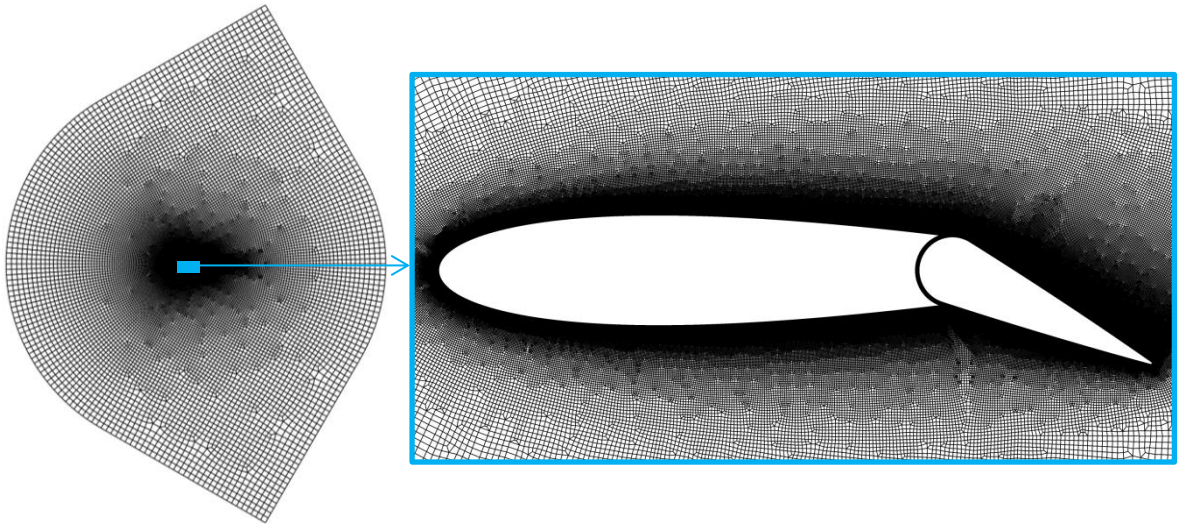

Figure 3 – Example of a computational 2D mesh

The flow was computed using ANSYS CFX for the solution of Reynolds-averaged Navier–Stokes equations. The shear stress transport k-ω turbulence model was used together with the γ laminar–turbulent transition model. The turbulence intensity computed at a distance of one-sixth of the airfoil chord to its leading edge corresponded to the experimental value of $Tu \approx 1.2\%$. To obtain $Re = 1.4 \times 10^6$, the computations were carried out at reduced pressure. For modeling the effect of wind-tunnel side walls, between which the wing was spanned, the inlet and outlet of the domain in 3D computations had the Nikuradse log-law velocity profile [9] in direction towards the side wall joined to the wing. Besides, this side wall had the no-slip condition while, for simplicity, the other wind-tunnel walls had the free-sleep condition.

The comparisons with the experimental data [1,2] for the dependencies of the drag coefficient C_D on the control-surface deflection angle δ at zero angle of attack are shown in Figures 4(a) and 4(b) for the 3D and 2D computations, respectively. The experimental data for the C_D were limited to $\delta = 15°$. In this δ range, the 3D and 2D computations produced close results. In the experiment for the range of small control-surface deflection angles, which is the most interesting for fuel burn reduction, the drag increase due to the installation of the control surface with the OB instead of the one with the PO was $\Delta C_D \approx 0.0022$ at $\delta = 0$ and $\Delta C_D \approx 0.0036$ at $\delta = 5°$. The same maximum increase $\Delta C_D \approx 0.0036$ was obtained in computations but at a smaller $\delta = 0$.

The computational 2D results showed satisfactory agreement with experimental data for the dependencies of the lift C_L and hinge moment C_h coefficients on the control-surface deflection angle δ at zero angle of attack, as can be seen in Figures 5(a) and 5(b), respectively. The $C_L(\delta)$ curves show somewhat greater effectiveness of the control surface with the PO compared to the one with the OB at small and moderate deflection angles up to $\delta \approx 15°$ in the experiment and $\delta \approx 10°$ in the computation. For the range of $\delta \approx 15 – 25°$ in the experiment and $\delta \approx 10 – 25°$ in the computation, the control surface with the OB was more effective than the one with the PO. After $\delta \approx 25°$ the control surface with the OB lost effectiveness while, for the control surface with the PO, the C_L grew steadily. The hinge moments of the control surface with the OB are significantly lower in absolute values than for the control surface with the PO in the entire investigated range of deflection angles (Figure 5(b)).

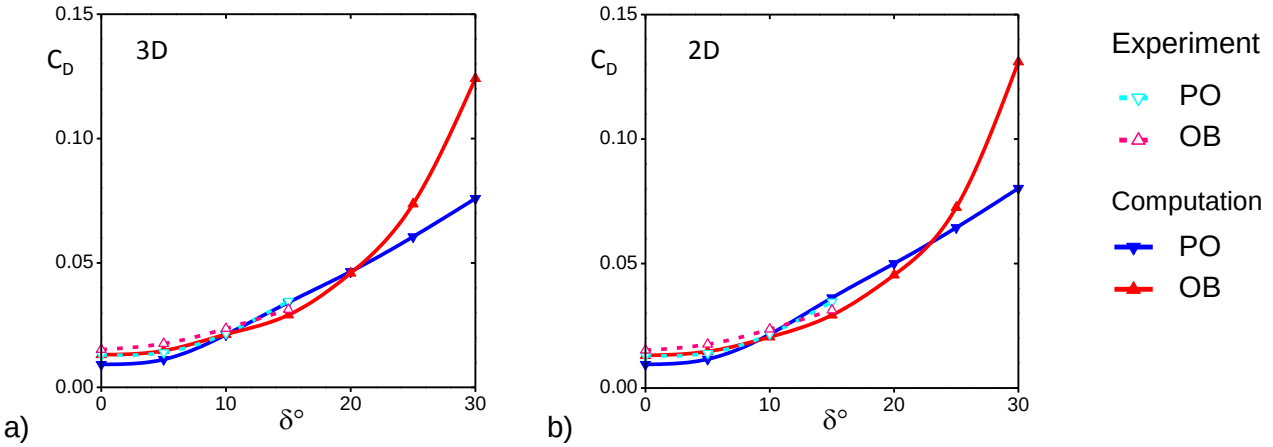

Figure 4 – Comparisons of the experimental drag coefficient with computational 3D (a) and 2D (b) results (Re = 1.4×10^6, Tu ≈ 1.2%, $\alpha = 0$).

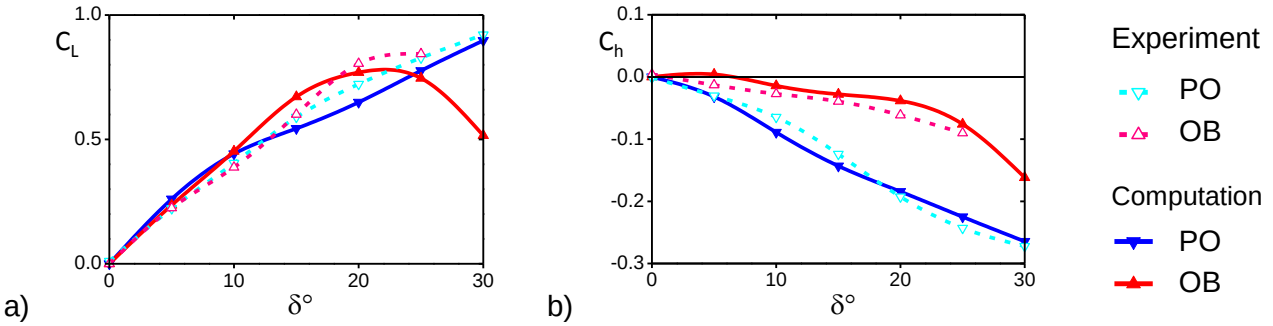

Figure 5 – Comparisons of the experimental lift (a) and hinge moment (b) coefficients with computational 2D results (Re = 1.4×10^6, Tu ≈ 1.2%, $\alpha = 0$).

The 2D computations of the external flow allow for the investigation of the effect of geometrical differences in aerodynamic surfaces without the interference of wind-tunnel effects, which are especially noticeable at large deflections of the control surfaces. That is why the further computational investigations of aerodynamic-surface modifications were conducted in 2D. For conciseness the aerodynamic surface in 2D computations will be further referred to as the airfoil.

4. Aerodynamic Effects for the Undeflected Control Surface

The airfoil modifications for the current investigations were limited to a short portion with the length of Δx_{mod} = 10% of the airfoil chord immediately ahead of the control surface (See Figure 1(c)). In the transverse direction, the airfoil was smoothly trimmed from both sides in the same way to the depth determined by the Δy_{mod} parameter.

Along with the flow simulation for the previously described selection of parameters with the wind-tunnel Reynolds number, Re = 1.4×10^6 (in accordance with [1,2]), computational studies were also carried out using the following incident flow parameters: M = 0.1, Re = 7×10^6, and Tu ≈ 0.2%. The turbulence intensity at the full-scale Reynolds number of Re = 7×10^6 was chosen taking into account the restrictions on the use of the γ laminar–turbulent transition model, according to which the condition Tu > 0.1% must be satisfied in the vicinity of the investigated surface.

The contours of the Mach number near the airfoil are shown in Figure 6 for Re = 7×10^6 and different values of Δy_{mod} together with the data for the basic versions of the airfoil with control surfaces. The proposed airfoil modification, with the appropriate depth (Δy_{mod}), led to a smaller zone of stagnant air near the leading edge of the control surface with the OB. It also reduced the boundary layer thickness on the control surface to the values more typical for the control surface with the PO.

The dependencies of the drag coefficient C_D on the airfoil modification depth Δy_{mod} (values at Δy_{mod} = 0 were obtained for the original airfoil) are shown in Figure 7 both for the full-scale and wind-tunnel conditions. The data for the control surface with the PO are also presented for comparison.

The values of $\Delta y_{mod} = 1 – 1.5\%$ of the airfoil chord are optimal in terms of decreasing the aerodynamic drag. At these values, the drag rise due to using the control surface with the OB instead of the PO became few times smaller.

The distribution of the computed pressure coefficient on the airfoils including the one with the optimal modification ($\Delta y_{mod} = 1.5\%$) is presented in Figure 8. At $\Delta y_{mod} = 1.5\%$ there is a noticeable pressure increase near the leading edge of the control surface with the OB followed by a larger pressure-drop zone. This effect is more obvious in the full-scale (Figure 8(a)) than in wind-tunnel (Figure 8(b)) conditions.

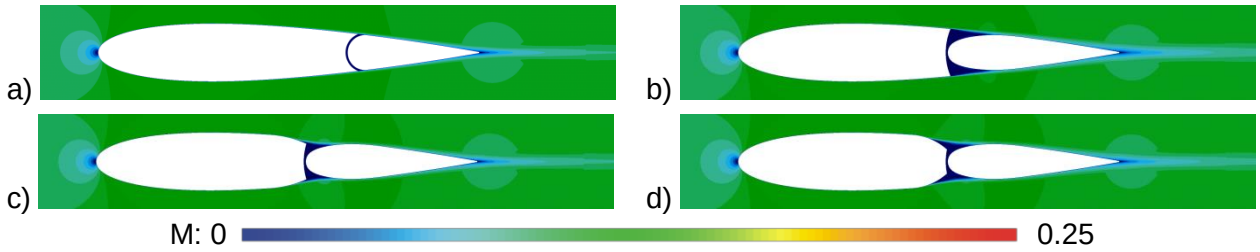

Figure 6 – Contours of Mach number near the versions of the airfoil with the control surfaces (Re = 7×10^6, Tu ≈ 0.2%, $\alpha = 0$, $\delta = 0$). For the original airfoil: control surface with PO (a) and OB (b). For the modified airfoil: control surface with OB, $\Delta y_{mod} = 1.5\%$ (c) and 3% (d).

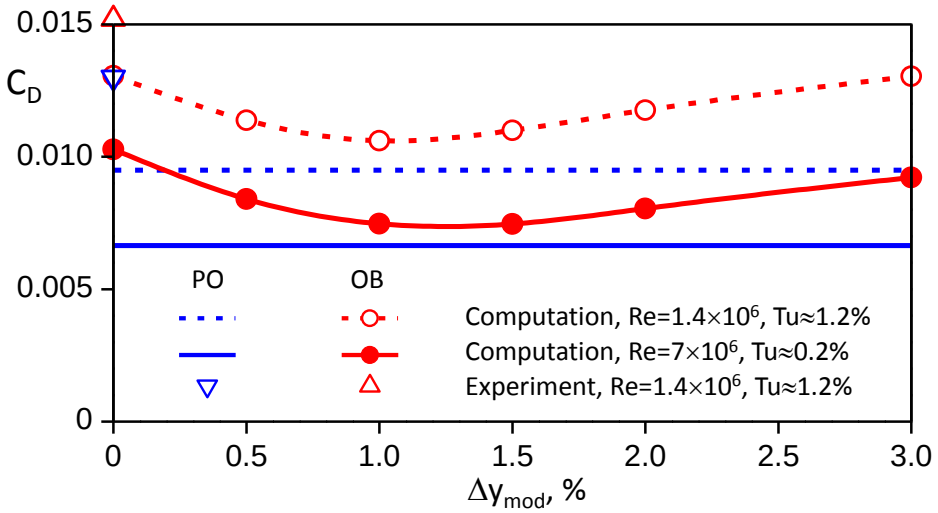

Figure 7 – Drag coefficient at $\alpha = 0$, $\delta = 0$.

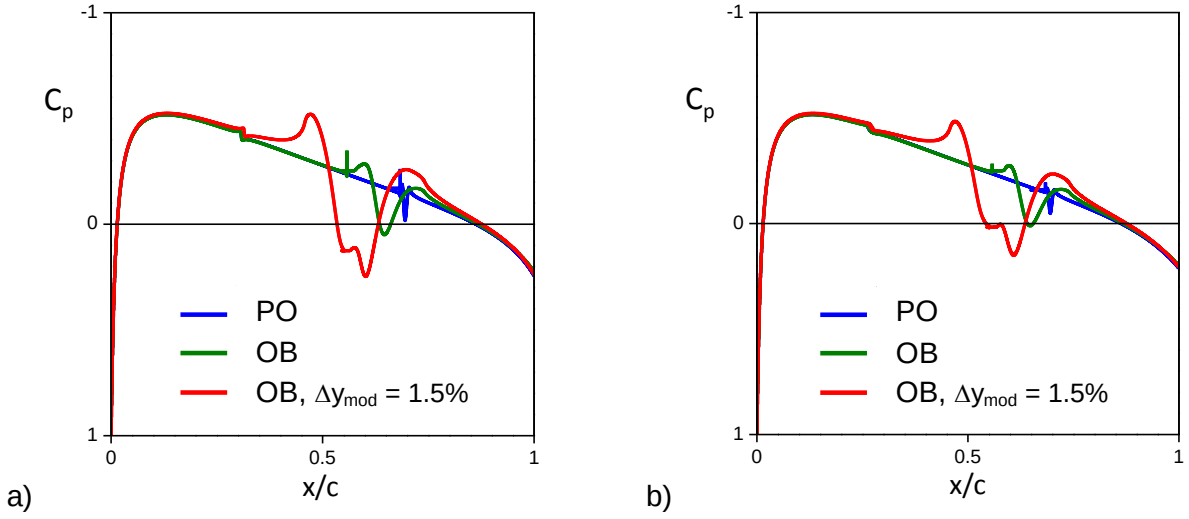

Figure 8 – Pressure coefficient at $\alpha = 0$, $\delta = 0$: (a) Re = 7×10^6, Tu ≈ 0.2%; (b) Re = 1.4×10^6, Tu ≈ 1.2%.

Positive aerodynamic effects are also revealed for the airfoil at incidence. For example at an angle of attack of α=15° in the full-scale conditions, it can be seen from the contours of the Mach number in Figure 9 that, while, for the original airfoil, the flow separation on the control surface with the OB (Figure 9(b)) is much more developed than for the control surface with the PO (Figure 9(a)), for the modified airfoil, the separation is somewhat reduced at Δy_{mod} = 1% (Figure 9(c)) and almost disappeared at Δy_{mod} = 3% (Figure 9(d)). For the greater modification depth, the stream ejected through the gap near the OB from the pressure to the suction side moves closer to the OB whereas, for the smaller modification depth or without it, this stream moves closer to the main airfoil.

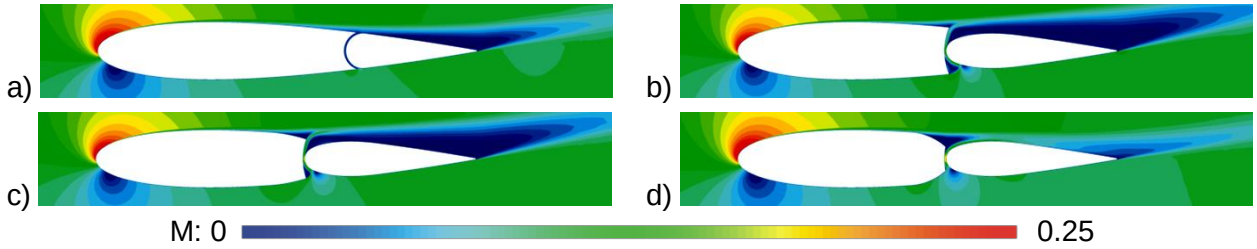

Figure 9 – Contours of Mach number near the versions of the airfoil with the control surfaces (Re = 7×10^6, Tu ≈ 0.2%, α = 15°, δ = 0). For the original airfoil: control surface with PO (a) and OB (b). For the modified airfoil: control surface with OB, Δy_{mod} = 1% (c) and 3% (d).

The reduced separation on the control surface contributed to higher lift and lower drag for the airfoil at incidence. The Figures 10(a) and 10(b) show the C_L-α and C_L-C_D curves in the full-scale conditions. The use of the OB resulted in significantly lower lift and higher drag compared to the use of the PO for the control surface of the original airfoil. Meanwhile, the airfoil modification improved the situation for the control surface with the OB. For the airfoil modification depth of Δy_{mod} = 1%, the improvement is relatively small but, at Δy_{mod} = 3%, the lift of the modified airfoil having the control surface with the OB reached the lift of the original airfoil having the control surface with the PO at α = 10° and exceeded it at greater angles of attack with comparable drag levels. It should be noted that, at Δy_{mod} = 1%, the drag of the modified airfoil is noticeably lower than at Δy_{mod} = 3% at zero angle of attack but, at α > 5°, the drag is lower for the greater modification depth.

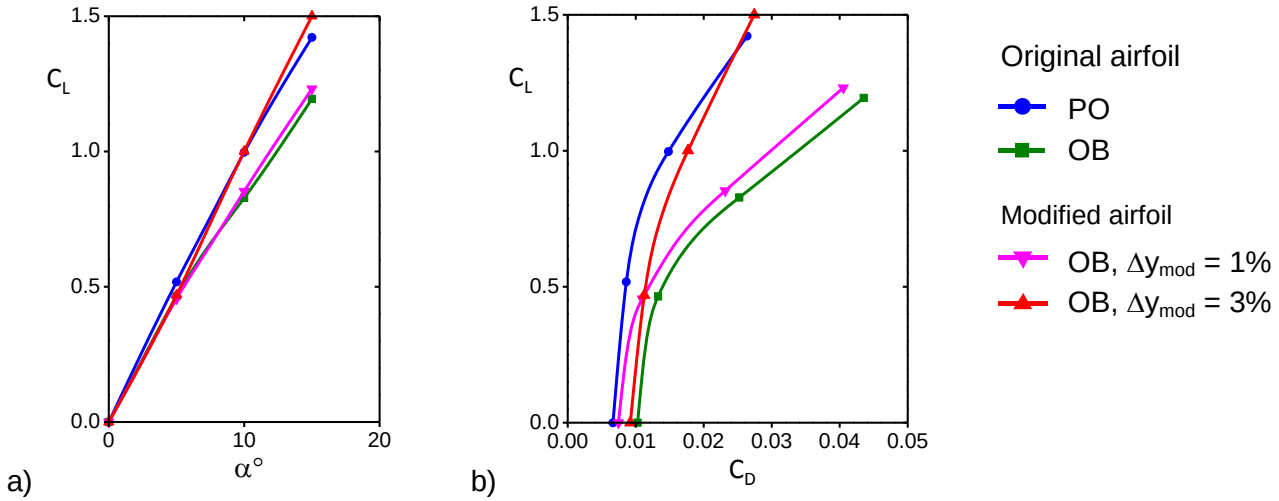

Figure 10 – C_L-α (a) and C_L-C_D (b) curves (Re = 7×10^6, Tu ≈ 0.2%, δ = 0).

5. Aerodynamic Effects for the Deflected Control Surface

Computational studies for the deflected control surface were carried out at a zero angle of attack. For the control-surface deflection angle of δ = 25° in the full-scale conditions, the contours of the Mach number near the airfoil are shown in Figure 11. For the original airfoil, there are large separation zones of close size on the control surface both with the PO and OB (Figures 11(a) and 11(b), respectively). For the modified airfoil, the separation zone is somewhat smaller at Δy_{mod} = 1%

(Figure 11(c)), but the modification effect is the most noticeable at Δy_{mod} = 3% (Figure 11(d)). In the last case the separation on the control surface is almost eliminated and there is extensive stream ejection from the pressure to the suction side through the wide gap near the OB.

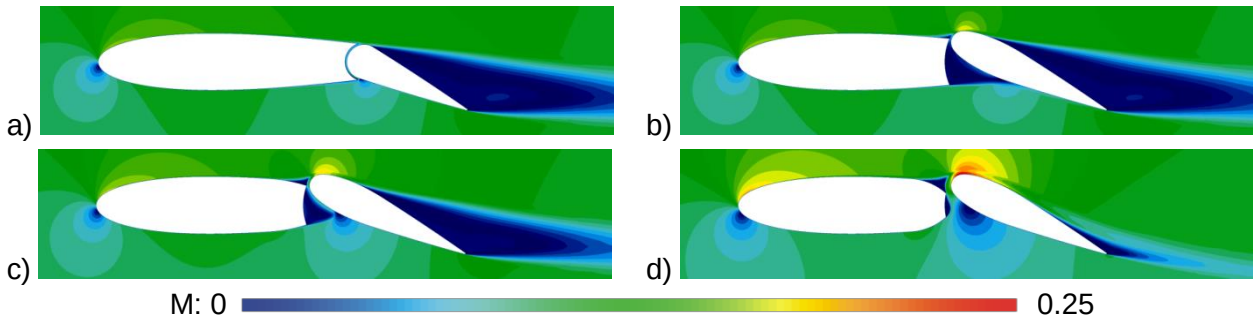

Figure 11 – Contours of Mach number near the versions of the airfoil with the control surfaces in full-scale conditions (Re = 7×10^6, Tu ≈ 0.2%, α = 0, δ = 25°). For the original airfoil: control surface with PO (a) and OB (b). For the modified airfoil: control surface with OB, Δy_{mod} = 1% (c) and 3% (d).

The same analysis was conducted in the wind-tunnel conditions, for which the contours of the Mach number are presented in Figure 12. In these conditions with the lower Reynolds number, the separation zones became larger, especially for the control surfaces with the OB on the original airfoil (Figure 12(b)) and on the modified airfoil at the small modification depth of Δy_{mod} = 1% (Figure 12(c)). The distinctive separation zone reduction is only noticeable at Δy_{mod} = 3% (Figure 12(d)).

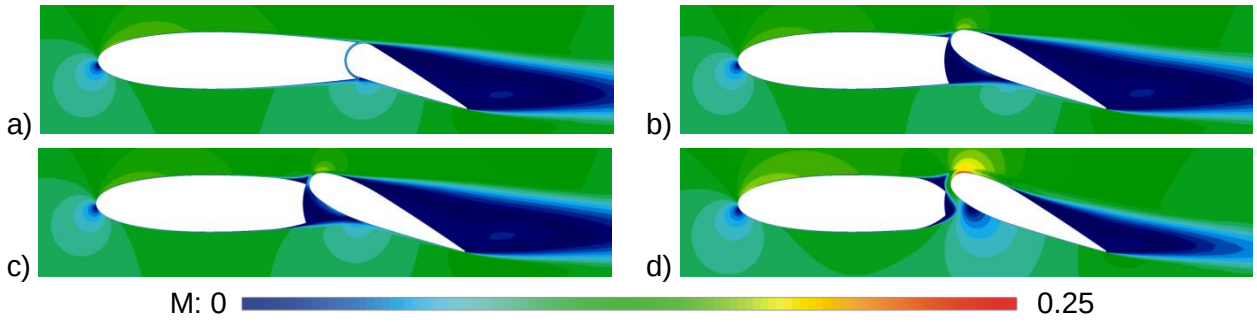

Figure 12 – Contours of Mach number near the versions of the airfoil with the control surfaces in wind-tunnel conditions (Re = 1.4×10^6, Tu ≈ 1.2%, α = 0, δ = 25°). For the original airfoil: control surface with PO (a) and OB (b). For the modified airfoil: control surface with OB, Δy_{mod} = 1% (c) and 3% (d).

The results of the pressure distribution computation on the original and modified airfoil having the control surface with the OB are presented in Figures 13(a) and 13(b) for the full-scale and wind-tunnel conditions, respectively. The control-surface deflection angle is of δ = 25°, which corresponds to Figures 11 and 12. In the full-scale conditions (Figures 13(a)), the airfoil modification at Δy_{mod} = 1% led to somewhat higher suction peak on the control surface and distinguished stagnation point on it with the pressure coefficient of $C_p \approx 1$. The rise of suction is also quite noticeable on the main airfoil. The similar but much more direct trends are seen at Δy_{mod} = 3%. Meanwhile in the wind-tunnel conditions (Figures 13(b)), the airfoil modification at Δy_{mod} = 1% resulted only in some local change in the pressure distribution. In these conditions, only the modification at Δy_{mod} = 3% produced noticeable but smaller than in the full-scale conditions effect.

The optimal values of the airfoil modification depth (Δy_{mod}) for the control-surface deflection angle of δ = 25° can be obtained from Figures 14(a) and 14(b) presenting the lift coefficient (C_L) and drag coefficient (C_D) dependencies on Δy_{mod}. These figures also show the levels of C_L and C_D for the original airfoil with the PO. For the full-scale conditions, the increase in the lift reached the flat maximum values of about 76% at more than halved drag in the range of Δy_{mod} = 2 – 3.5%. For the wind-tunnel conditions, the optimum Δy_{mod} = 3% and the increase in the lift was only about 43%.

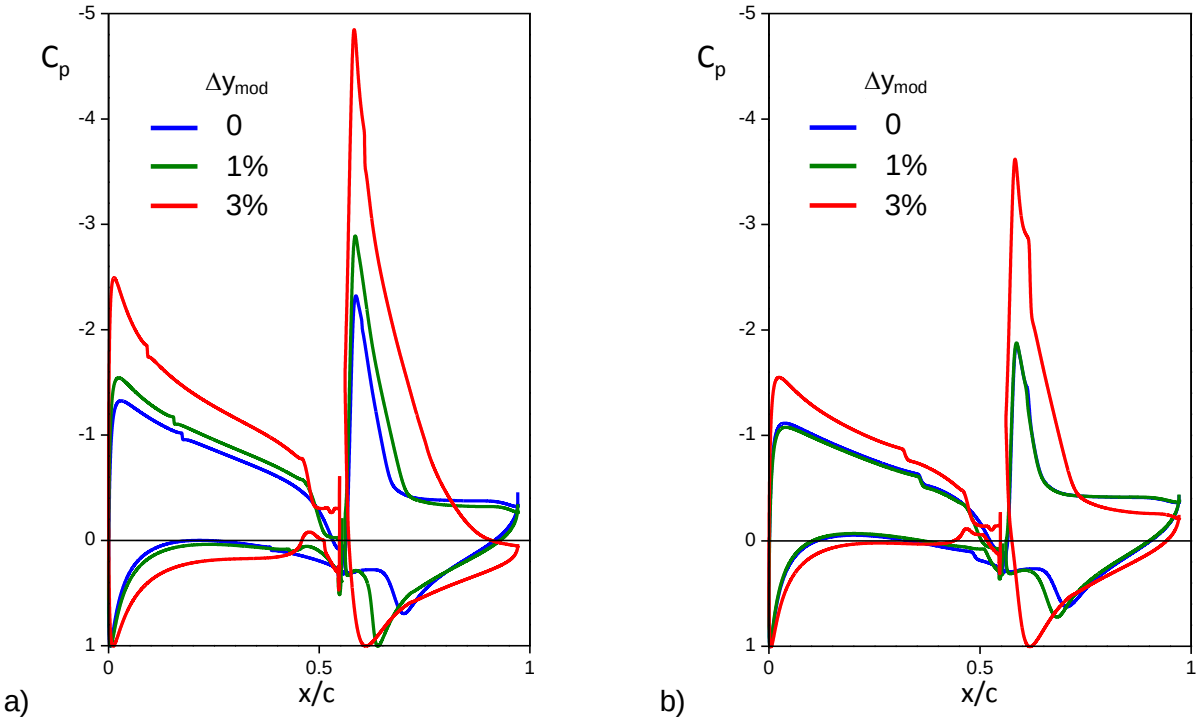

Figure 13 – Pressure coefficient at $\alpha = 0$, $\delta = 25°$ for the control surface with the OB on the original ($\Delta y_{mod} = 0$) and modified ($\Delta y_{mod} = 1$ and 3%) airfoils: (a) Re = 7×10^6, Tu ≈ 0.2%; (b) Re = 1.4×10^6, Tu ≈ 1.2%.

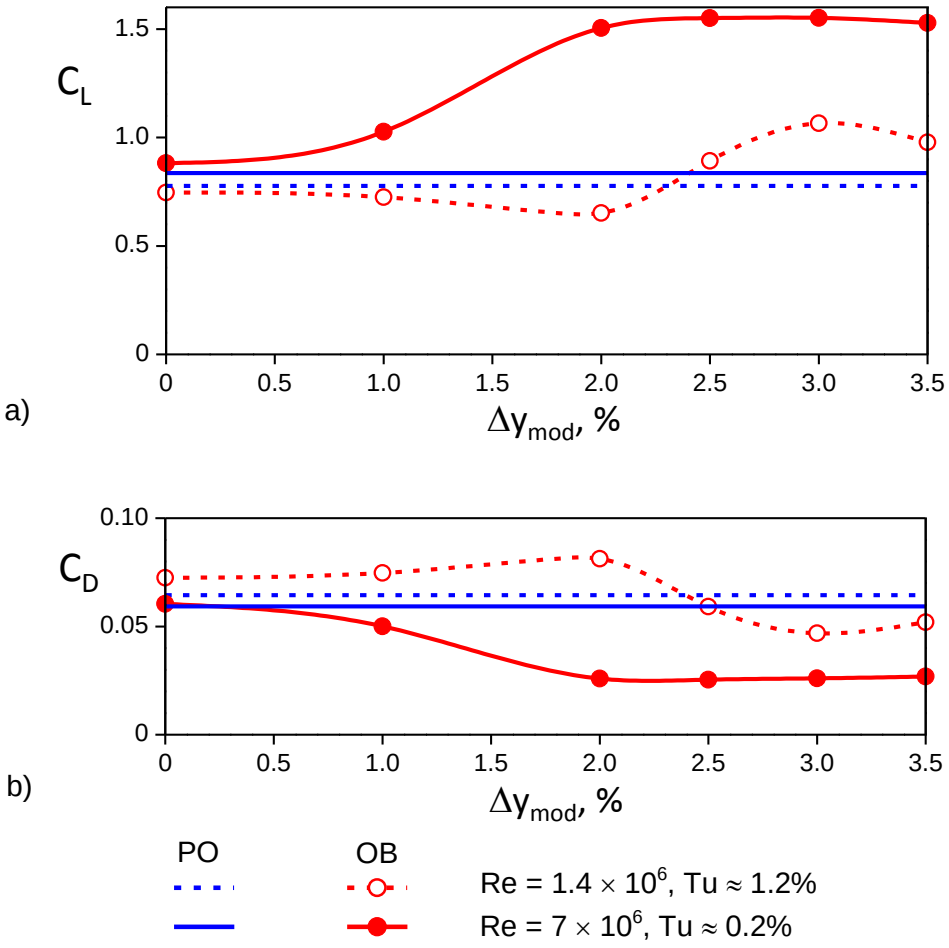

Figure 14 – Lift (a) and drag (b) coefficients at $\alpha = 0$, $\delta = 25°$.

The dependencies of the aerodynamic coefficients on the deflection angle of the control surface with the OB are compared in Figure 15 for the modified airfoil at Δy_{mod} = 1%, 2%, and 3%, and for its original version both in the full-scale and wind-tunnel conditions. The dependencies are also given for the deflection of the control surface with the PO. It can be seen that the airfoil modification significantly improved the effectiveness of the control surface with the OB and reduced the drag in the full-scale conditions (Re = 7×10^6, Tu ≈ 0.2%). The similar effects are noticeably weaker in the wind-tunnel conditions (Re = 1.4×10^6, Tu ≈ 1.2%) and are most pronounced for the sufficiently large modification at Δy_{mod} = 3%.

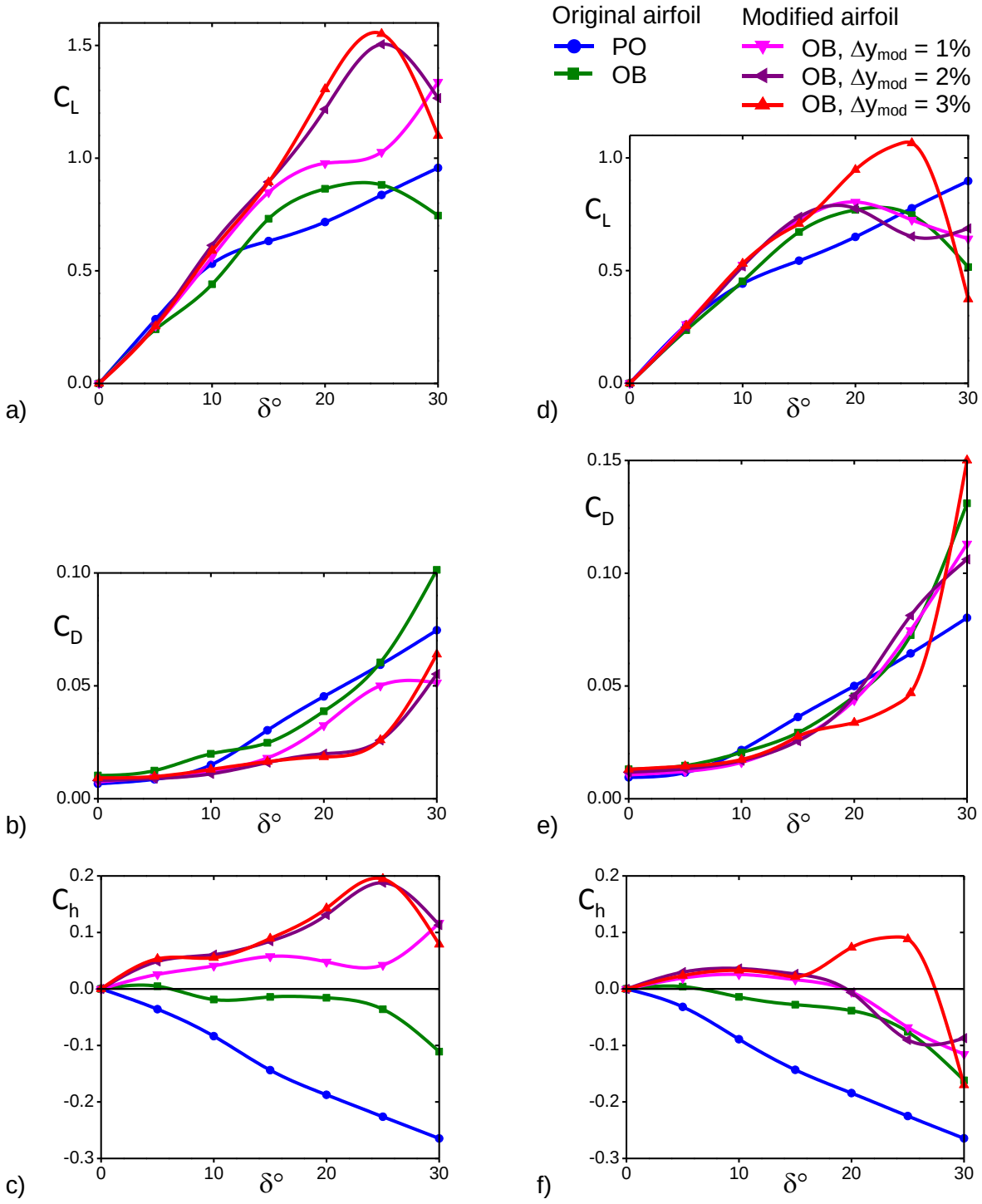

Figure 15 – Lift (C_L), drag (C_D), and hinge moment (C_h) coefficients at $\alpha = 0$ for Re = 7×10^6, Tu ≈ 0.2% (a – c) and Re = 1.4×10^6, Tu ≈ 1.2% (d – f).

The investigated modifications to the airfoil also significantly changed the dependencies of the control-surface hinge moments on its deflection angle (Figures 15(c) and 15(f)). There is an obvious trend for the overbalancing of the control surface with the OB especially in the full-scale conditions. The problem of overbalancing can be solved by the use of anti-servo tabs, which may also produce an additional increment in the control-surface effectiveness, or by the partial balancing of the control surface when only the part of its span has an OB. Moreover, the control-surface overbalancing may be acceptable for the irreversible powered control systems and UAVs.

The more radical way of changing the hinge moments is the proper choice of an OB shape and of a control-surface hinge-line position. The choice of the OB shape is a separate task but some investigations of the change in the control-surface hinge-line position without reshaping the OB are also outlined in the current paper. The dependency of the hinge moment coefficient (C_h), for the control surface deflected to an angle of $\delta = 25°$, on the hinge-line position ($x_{H.L}$) is presented in the Figure 16 for the modified airfoil at the modification depth of $\Delta y_{mod} = 3\%$ in the full-scale conditions. The original hinge-line position corresponds to $x_{H.L} = 70\%$ of the airfoil chord. The hinge moment close to zero was obtained at $x_{H.L} = 67.7\%$. The shift in the hinge line position from $x_{H.L} = 70\%$ to 66.7% did not particularly influenced the flow pattern as can be seen in Figure 17 where the contours of the Mach number are shown and the positions of the hinge line are marked with a cross.

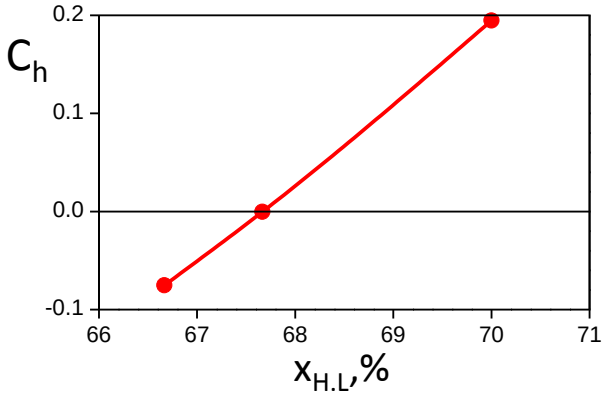

Figure 16 – Hinge moment coefficient at $\alpha = 0$, $\delta = 25°$, $\Delta y_{mod} = 3\%$ ($Re = 7 \times 10^6$, $Tu \approx 0.2\%$).

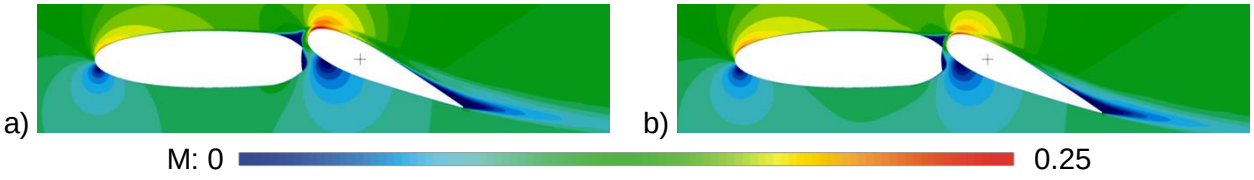

Figure 17 – Contours of Mach number near the modified airfoil ($\Delta y_{mod} = 3\%$) for the control surface with the original (a) and shifted to $x_{H.L} = 66.7\%$ (b) hinge line ($Re = 7 \times 10^6$, $Tu \approx 0.2\%$, $\alpha = 0$, $\delta = 25°$).

The computations conducted for the modified airfoil at $\Delta y_{mod} = 3\%$ with the control-surface hinge line shifted to $x_{H.L} = 67.7\%$ resulted in very small hinge moments of the control surface with the OB in the entire investigated range of the control-surface deflection angles. What is more, the shift in the hinge-line position also caused some increment in the control-surface effectiveness. The corresponding results of the hinge-moment (C_h) and lift (C_L) coefficient computations in comparison with the ones for the original hinge-line position are presented in Figure 18.

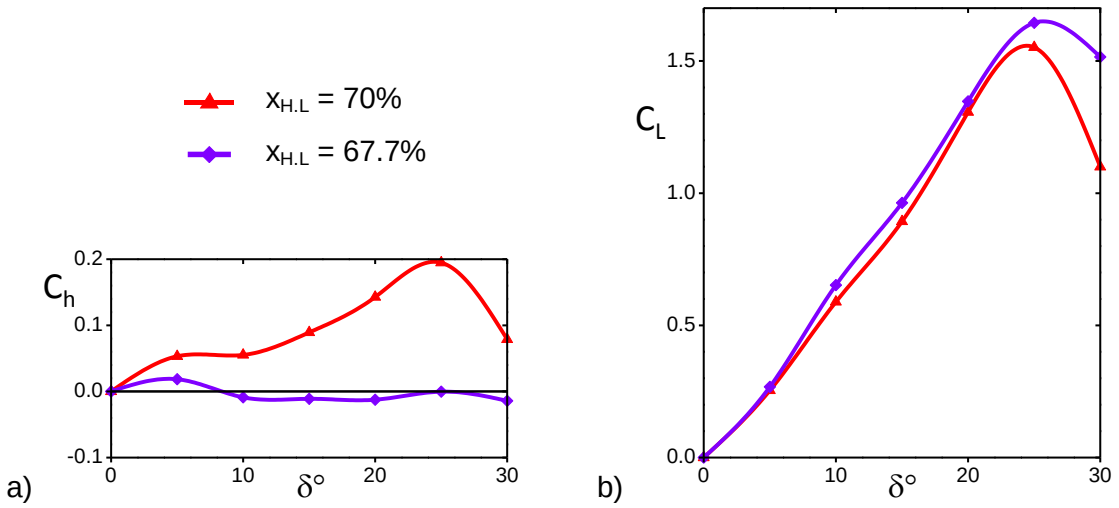

Figure 18 – Hinge moment (a) and lift (b) coefficients for different hinge line positions at the airfoil modification depth of Δy_{mod} = 3% (Re = 7 × 10^6, Tu ≈ 0.2%, α = 0).

Conclusion

The conducted numerical researches showed that small changes in the shape of an aerodynamic surface ahead of an aerodynamically balanced control surface can improve both the aerodynamic-surface aerodynamic perfection and control-surface effectiveness. The results of the investigations are presented concerning the aerodynamic characteristics of the aerodynamic surface with a NACA 0015 airfoil modified by its symmetric trimming limited by the depth of Δy_{mod} and length of Δx_{mod} immediately ahead of the control surface. For the current research the modification length was fixed at Δx_{mod} = 10% of the airfoil chord.

According to the 2D CFD analysis for the aerodynamic surface at zero angle of attack, the appropriate airfoil modification depth (Δy_{mod}) led to a smaller zone of stagnant air near the leading edge of the control surface at zero deflection angle. The values of Δy_{mod} = 1 – 1.5% of the airfoil chord were optimal in terms of decreasing the aerodynamic drag. At these values, the drag rise due to using the aerodynamically balanced control surface instead of a simple one decreased by 3.3 – 4.5 times, depending on the Reynolds number. Furthermore, at increased angles of attack, the computations showed the higher lift and lower drag of the aerodynamic surface with the undeflected control surface due to the airfoil modification.

The 2D CFD analysis also indicated that for the deflected control surface the airfoil modification can significantly change the flow pattern substantially reducing the separation zone on the control surface. The positive effect of the airfoil modification on the control-surface effectiveness is especially pronounced at Reynolds numbers close to the full-scale ones. For instance, at the control-surface deflection angle of δ = 25°, zero angle of attack, and Re = 7 × 10^6, the lift increased by approximately 70 – 75% for the modification depth of Δy_{mod} = 2 – 3.5%. At Re = 1.4 × 10^6, which is typical for testing models in small wind tunnels at atmospheric pressure, the airfoil modification affected the control surface effectiveness much less and, at zero angle of attack, led to a maximum increase in the lift only by about 43% at Δy_{mod} = 3%.

In accordance with the computational results the proposed airfoil modification caused the overbalancing of the control surface. The overbalancing may be eliminated, for instance, by anti-servo tabs, which may also additionally increase the control-surface effectiveness, or by aerodynamic balancing of the control surface only on the part of its span. On the other hand the overbalancing may be acceptable for the irreversible powered control systems or UAVs.

The aerodynamic-balance shape and the control-surface hinge-line position modifications are also among the direct ways of influencing the hinge moments. The aerodynamic-balance shape choice is a separate task but the computational researches showed that a simple shift of the hinge line upstream by 2.3% of the airfoil chord essentially eliminated the overbalancing of the investigated control surface on the modified airfoil at Δy_{mod} = 3% and additionally increased the control-surface effectiveness.

To summarize, the proposed modification of the aerodynamic-surface airfoil can be advantageous both for the cruise flight with undeflected control surfaces and for the flight modes that require effective control including emergencies such as one engine-out case. Moreover, the considered modification can be adapted for the use with unpowered or low-power control systems.

References

[1] Sears R I and Liddell R B. Wind-tunnel investigations of control-surface characteristics VI: A 30-percent-chord plain flap on the NACA 0015 airfoil. NACA WR-L-454, 1942.

[2] Sears R I and Gillis C L. Wind-tunnel investigations of control-surface characteristics VIII: A large aerodynamic balance of two nose shapes used with a 30-percent-chord flap on an NACA 0015 airfoil. NACA WR-L-378, 1942.

[3] Andreev G T , Glushchenko G N, Kutukhina N V , Mel'nichuk Yu P, and Pavlenko O V. *Aerodynamic compensation of hinge moments for the unpowered airplane controls.* Moscow: Innovatcionnoe Mashinostroenie (Innovative Engineering), 2017 (in Russian).

[4] Bogatyrev V V. Numerical investigations of the effects of shapes and sizes of the gap between the lifting surface and control surface with the overhang balance on its effectiveness and hinge moment. *TsAGI Sci J*, vol. 48, no. 1, pp 10-20, 2017.

[5] Bogatyrev V V. Russian Federation patent 2675304, 2018.

[6] Bogatyrev V V. The method of decreasing the aerodynamic drag of a lifting surface equipped with the aerodynamically balanced control surface. *Proc of 30th Science-Technical Conference on Aerodynamics*, Volodarskogo, pp 57–58, 2019 (in Russian).

[7] Repik E U and Sosedko Yu P. The flow turbulence influence on the results of tests in wind tunnels. *Uch Zap TsAGI*, vol. 24, No. 3, pp 76–90, 1993 (in Russian).

[8] Repik E U and Sosedko Yu P. *The flow turbulence level control*. Moscow: Fizmatlit, 2002 (in Russian).

[9] Nikuradse J. Laws of flow in rough pipes. *VDI Forschungsheft* 361, 1933. In translation, NACA TM 1292, 1950.

Contact Author Email Address

Vladimir Bogatyrev, mailto: vladimir.bogatyrev@tsagi.ru

Copyright Statement